J|A|C|S
ARTICLES
Published on Web 02/22/2002

Product Binding to the Diiron(III) and Mixed-Valence Diiron Centers of Methane Monooxygenase Hydroxylase Studied by ^{1,2}H and ^{19}F ENDOR Spectroscopy

Stoyan K. Smoukov,[†] Daniel A. Kopp,[‡] Ann M. Valentine,[‡] Roman Davydov,[†] Stephen J. Lippard,*[,‡] and Brian M. Hoffman*[,†]

Contribution from the Department of Chemistry, Northwestern University,[†] Evanston, Illinois 60208 and the Massachusetts Institute of Technology,[‡] Cambridge, Massachusetts 02139

Received January 16, 2001

Abstract: The binding of ethanol and 1,1,1-trifluoroethanol (TFE) to both the H_{mv} and H_{ox} forms of soluble methane monooxygenase (sMMO) in solution has been studied by Q-band (35 GHz) CW and pulsed ENDOR spectroscopy of ^{1}H, ^{2}H and ^{19}F nuclei of exogenous ligands. As part of this investigation we introduce ^{19}F, in this case from bound TFE, as a new probe for the binding of small molecules to a metalloenzyme active site. The H_{mv} form was prepared in solution by chemical reduction of H_{ox}. For study of H_{ox} itself, frozen solutions were subjected to γ-irradiation in the frozen solution state at 77 K, which affords an EPR-visible mixed-valent diiron center, denoted $(H_{ox})_{mv}$, held in the geometry of the diiron(III) state. The ^{19}F and ^{2}H ENDOR spectra of bound TFE together with ^{1,2}H ENDOR spectra of bound ethanol indicate that the alcohols bind close to the Fe(II) ion of the mixed-valence cluster in H_{mv} and in a bridging or semi-bridging fashion to H_{ox}. DMSO does not affect the binding of either of the ethanols or of methanol to H_{ox}, nor of ethanol or methanol to H_{mv}. It does, however, displace TFE from the diiron site in H_{mv}. These results provide the first evidence that crystal structures of sMMO hydroxylase into which product alcohols were introduced by diffusion represent the structures in solution.

Introduction

The oxidation of methane to methanol catalyzed by the soluble methane monooxygenase (sMMO)[1] enzyme systems of *Methylococcus capsulatus* (Bath) and *Methylosinus trichosporium* OB3b has been studied extensively.[2,3] Interest in these systems remains high to obtain a better understanding of the dioxygen and C−H bond activation steps and to provide an efficient low-temperature conversion of methane to methanol on an industrial scale.[4]

Methane monooxygenase catalyzes the first step in the metabolic pathway of methanotrophic bacteria, according to eq 1.

$$CH_4 + O_2 + NADH + H^+ \rightarrow CH_3OH + H_2O + NAD^+ \quad (1)$$

sMMO from *M. capsulatus* (Bath) has three protein components required for activity, a 251 kDa hydroxylase, a 38.5 kDa reductase, and a 15.9 kDa coupling protein. The hydroxylase component, an $\alpha_2\beta_2\gamma_2$ dimer, contains a non-heme dinuclear iron center in each of its two α subunits. The reduced diiron(II) form of the enzyme reacts with dioxygen to produce a high-valent iron intermediate that reacts with methane and a variety of other substrates, including alkanes up to C_8, alkenes, aromatics, and haloalkanes.[5−8]

Structural studies of the hydroxylase component by X-ray crystallography have revealed the geometry of the active site in both the resting diiron(III) and diiron(II) states, as well as the mixed-valent Fe(II)Fe(III) state.[9−12] Kinetic and spectroscopic measurements have elucidated the nature of intermediates in the reaction of MMOH with dioxygen.[13−16] Electron−nuclear

[†] Northwestern University.
[‡] Massachusetts Institute of Technology.

(1) List of abbreviations: sMMO, soluble methane monooxygenase; MMOH, hydroxylase component of sMMO; H_{mv}, mixed-valent Fe(II)Fe(III) MMOH; H_{ox}, oxidized (diiron(III)) MMOH; $[H_{ox}]_{mv}$, mixed-valent MMOH produced by cryoreduction of H_{ox}; TFE, 1,1,1-trifluoroethanol, also used to refer to CF_3CH_2OH and CF_3CD_2OH collectively when the ^{2}H label is of no significance.

(2) (a) Valentine, A. M.; Lippard, S. J. *J. Chem. Soc., Dalton Trans.* **1997**, 3925−3931. (b) Merkx, M.; Kopp, D. A.; Sazinsky, M. H.; Blazyk, J. L.; Muller, J.; Lippard, S. J. *Angew. Chem. Int. Ed.* **2001**, *40*, 2782−2807.
(3) Wallar, B. J.; Lipscomb, J. D. *Chem. Rev.* **1996**, *96*, 2625−2657.
(4) Furuto, T.; Takeguchi, M.; Okura, I. *J. Mol. Catal. A: Chem.* **1999**, *144*, 257−261.
(5) Colby, J.; Stirling, D. I.; Dalton, H. *Biochem. J.* **1977**, *165*, 395−402.
(6) Dalton, H.; Golding, B. T.; Waters, B. W.; Higgins, R.; Taylor, J. A. *J. Chem. Soc., Chem. Commun.* **1981**, 482−483.
(7) Fox, B. G.; Dege, J. E.; Froland, W. A.; Lipscomb, J. D. *J. Biol. Chem* **1989**, *264*, 10023−10033.
(8) Liu, K. E.; Lippard, S. J. In *Advances in Inorganic Chemistry*; Sykes, A. G., Ed.; Academic Press: San Diego, 1995; Vol. 42, pp 263−289.
(9) Rosenzweig, A. C.; Frederick, C. A.; Lippard, S. J.; Nordlund, P. R. *Nature* **1993**, *366*, 537−543.
(10) Rosenzweig, A. C.; Nordlund, P.; Takahara, P. M.; Frederick, C. A.; Lippard, S. J. *Chem. Biol.* **1995**, *2*, 409−418.
(11) Rosenzweig, A. C.; Brandstetter, H.; Whittington, D. A.; Nordlund, P.; Lippard, S. J.; Frederick, C. A. *Proteins: Struct., Funct., Genet.* **1997**, *29*, 141−152.
(12) Whittington, D. A.; Lippard, S. J. *J. Am. Chem. Soc.* **2001**, *123*, 827−838.
(13) Lee, S. K.; Nesheim, J. C.; Lipscomb, J. D. *J. Biol. Chem.* **1993**, *268*, 21569−21577.
(14) Liu, K. E.; Valentine, A. M.; Wang, D.; Huynh, B. H.; Edmondson, D. E.; Salifoglou, A.; Lippard, S. J. *J. Am. Chem. Soc.* **1995**, *117*, 10174−10185.
(15) Valentine, A. M.; Stahl, S. S.; Lippard, S. J. *J. Am. Chem. Soc.* **1999**, *121*, 3876−3887.

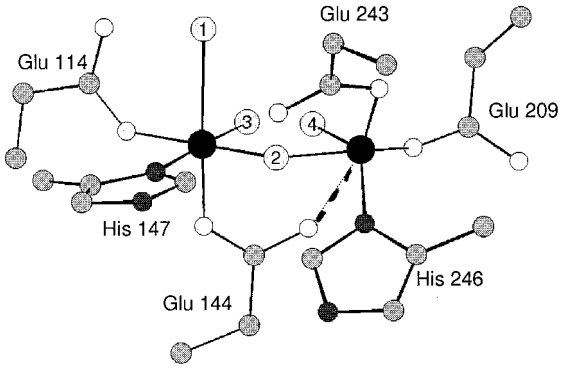

Figure 1. A representation of the MMOH active site based on the crystal structure of $MMOH_{mv}$; the actual cluster is highly flexible, adopting a variety of structures associated with shifts of the carboxylate of Glu243.[12] Black spheres represent iron; light gray spheres, carbon; dark gray spheres, nitrogen; unfilled spheres, oxygen. Numbered positions represent known sites for binding exogenous ligands.

double resonance (ENDOR) spectroscopy serves as an important complement to X-ray crystallographic techniques in the study of metalloenzymes.[17] Its use in the study of sMMO has primarily been to investigate the binding of exogenous ligands to the available sites of the diiron center, Figure 1. Early studies established the presence of a hydroxo bridge and characterized the binding of DMSO in the paramagnetic, mixed-valence, Fe(II)Fe(III) state of the cluster,[18] denoted H_{mv}, in which $S = 2$ and $S = {}^5/_2$ centers couple antiferromagnetically to give a ground-state spin of ${}^1/_2$.

Knowledge of the substrate- or product-bound states of the enzyme provides valuable clues for unraveling details of the MMOH catalytic mechanism. A previous ENDOR study revealed that methanol coordinates to chemically prepared H_{mv}.[19] The only spectroscopic evidence for the binding of this product alcohol to the *oxidized* diiron(III) center came through examination[20] of samples of the frozen methanol and phenol complexes of the EPR-silent diiron(III) form (H_{ox}) that had been radiolytically cryoreduced.[21] This technique yields an EPR-visible mixed-valence state, denoted $(H_{ox})_{mv}$, that maintains the geometry of the precursor diferric cluster. When H_{ox} binds an alcohol or other small molecule, the cryoreduced state is designated (H_{ox} + alcohol)$_{mv}$. Dramatic differences between the EPR spectra of (H_{ox} + methanol)$_{mv}$ and of $(H_{ox})_{mv}$ disclosed ligation of the alcohol to the diiron(III) active site.[20]

In the present work we have investigated the interactions of ethanol and 1,1,1-trifluoroethanol (TFE) with both the H_{mv} and H_{ox} forms of sMMO in solution by Q-band (35 GHz) CW and pulsed ENDOR spectroscopy of ^{1}H, ^{2}H, and ^{19}F nuclei. As part of this study we introduce ^{19}F, in this case from bound TFE, as a new probe for the binding of small molecules to a metalloenzyme active site. This approach is most favorably applied when the ENDOR measurements are made at 35 GHz or higher frequency. These measurements have been carried out in parallel with, and are discussed in terms of, the crystallographic studies of H_{mv}[12] and of alcohol binding to H_{ox}.[22] The crystal structures have led us to reinvestigate the ENDOR signals from the exchangeable protons of water bound to the mixed-valence diiron center both in the presence and absence of bound alcohol. The combined results suggest that alcohols bind differently to H_{ox} than to H_{mv}, permit a unified model for product binding to the enzyme, and confirm that the structures of the enzyme with product alcohols introduced by diffusion into preformed crystals are consistent with the structures in solution.

Experimental Section

Protein Purification and Sample Preparation. MMOH was purified from *M. capsulatus* (Bath) with the iron content and activity as reported previously.[23] Chemical reduction to the H_{mv} state was accomplished as described elsewhere.[19] In brief, the protein was concentrated to ~1 mM by ultrafiltration, mixed with an equimolar amount of electron-transfer mediators (phenazine methosulfate, potassium indigo tetrasulfonate, and methylene blue), and reduced with sodium dithionite. Small molecules were added prior to reduction to a final concentration of ~1 M. At 1 M concentration, ethanol is almost certain to inhibit activity, since it is a product and binds to the active site. A crystal structure of MMOH determined following a 1 M EtOH soak[22] reveals that the native structure is unperturbed, other than alcohol binding to the active site. Ethanol is also a substrate of the sMMO system, yielding acetaldehyde. Samples were allowed to equilibrate with the mediator solution for 1 h before being loaded in Q-band sample tubes and frozen. Samples of H_{ox} were similarly concentrated, mixed with small molecule, loaded in an EPR tube, and frozen prior to cryoreduction. Cryoreduction by γ-irradiation at 77 K to form EPR-visible $(H_{ox})_{mv}$ states was performed as described.[20]

Samples were prepared in the equilibrium mixed-valence H_{mv} form either by equilibration of $(H_{ox})_{mv}$ at ambient temperature[20] or by chemical reduction. The two kinds of preparations yielded equivalent ENDOR signals. Most data displayed were collected by the former method, which afforded 2−3 times greater EPR, and therefore ENDOR, intensities.

ENDOR Spectroscopy. Previously described 35 GHz continuous wave (CW)[24] and pulsed[25] ENDOR instrumentation and procedures were applied. CW 100 kHz, rapid passage absorption spectra were recorded at 2 K. All ENDOR signals displayed here arise from nuclei with Larmor frequencies $\nu > A/2$, which in a single-crystal spectrum consists of a doublet centered at the Larmor frequency and split by the hyperfine interaction, A. ^{2}H signal peaks are further split or broadened by the nuclear quadrupole interaction.

The Mims three-pulse[26,27] and Re-Mims four-pulse[28] techniques were used to collect pulsed ENDOR spectra. The Mims technique utilizes a three-pulse electron spin−echo sequence ($t_p - \tau - t_p - T - t_p - \tau -$ echo) and the Re-Mims sequence utilizes a four-pulse sequence ($t_p - \tau_1 - t_p - T - t_p - \tau_2 - 2t_p - (\tau_1 + \tau_2) -$ echo), where t_p is the microwave pulse width; the rf pulse is inserted during the interval, T. For a signal characterized by a hyperfine constant, A, the Mims and Re-Mims pulsed ENDOR techniques have a response R that depends on the product, $A\tau$ ($A\tau_1$ for Re-Mims), according to eq 2. This function has zeroes (hyperfine "suppression holes") at $A\tau = n$; $n = 0, 1, ...$, and

$$R \propto [1 - \cos(2\pi A\tau)] \qquad (2)$$

(16) Shu, L.; Nesheim, J. C.; Kauffman, K.; Munck, E.; Lipscomb, J. D.; Que, L. *Science* **1997**, *275*, 515−518.
(17) DeRose, V. J.; Hoffman, B. M. In *Methods in Enzymology*; Sauer, K., Ed.; Academic Press: New York, 1995; Vol. 246, pp 554−589.
(18) DeRose, V. J.; Liu, K. E.; Lippard, S. J.; Hoffman, B. M. *J. Am. Chem. Soc.* **1996**, *118*, 121−134.
(19) Willems, J.-P.; Valentine, A. M.; Gurbiel, R.; Lippard, S. J.; Hoffman, B. M. *J. Am. Chem. Soc.* **1998**, *120*, 9410−9416.
(20) Davydov, R.; Valentine, A. M.; Komar-Panicucci, S.; Hoffman, B. M.; Lippard, S. J. *Biochemistry* **1999**, *38*, 4188−4197.
(21) Davydov, R.; Kuprin, S.; Graslund, A.; Ehrenberg, A. *J. Am. Chem. Soc.* **1994**, *116*, 11120−11128.
(22) Whittington, D. A.; Sazinsky, M. H.; Lippard, S. J. *J. Am. Chem. Soc.* **2001**, *123*, 1794−1795.
(23) Gassner, G. T.; Lippard, S. J. *Biochemistry* **1999**, *38*, 12768−12785.
(24) Werst, M. M.; Davoust, C. E.; Hoffman, B. M. *J. Am. Chem. Soc.* **1991**, *113*, 1533−1538.
(25) Davoust, C. E.; Doan, P. E.; Hoffman, B. M. *J. Magn. Reson.* **1996**, *119*, 38−44.
(26) Mims, W. B. *Proc. R. Soc. London* **1965**, *283*, 452−457.
(27) Gemperle, C.; Schweiger, A. *Chem. Rev.* **1991**, *91*, 1481−1505.
(28) Doan, P. E.; Hoffman, B. M. *Chem. Phys. Lett.* **1997**, *269*, 208−214.

maxima at $A\tau = (2n + 1)/2$; $n = 0, 1, ...$ Such hyperfine selectivity is very useful in cases when signals from different nuclear species overlap. Here, we have used this property to help distinguish between ^{19}F and ^{1}H signals. On the 35 GHz pulsed ENDOR instrument, however, cavity ringdown limited experiments to ones with $\tau > 300-350$ ns; where shorter values of τ were necessary, the Re-Mims sequence was used. The Re-Mims gives results equivalent to those of the Mims sequence, but it is independent of instrumental deadtime limitations.

For a nucleus (n) of a ligand coordinated terminally to one iron (i) of an exchange-coupled diiron center ($i = 1, 2$), the hyperfine tensor arising from dipolar coupling to the mixed-valence cluster with modest g-anisotropy has the simple axial form shown by a nucleus bound to a mononuclear site,

$$\mathbf{A}_i^{(n)} = \mathbf{T}_i^{(n)}[-1, -1, 2] \qquad (3)$$

$$\mathbf{T}_i^{(n)} = K_i^{(n)} \times \frac{t^{(\mathbf{n})}}{r_i^{(n)}}$$

where the unique axis for the tensor **A** lies along the vector between the nucleus (n) and the Fe to which it is bound. The scale factor, $T_i^{(n)}$, is the product of three factors: one is the inverse cube of the Fe$_i$-n distance (r_i); the second, $t(n)$ is a product of fundamental constants and is specific to each nucleus; the third is a vector-coupling coefficient for Fe$_i$, K_i, which is determined by the spin-coupling scheme for the cluster. For convenience we list the $t(n)$ constants for several nuclei of interest in a spin-coupled cluster with total spin $S = {}^1/_2$, comprising an Fe^{3+} ($S = {}^5/_2$) antiferromagnetically coupled to an Fe^{2+} ($S = 2$) comprising.

$$t(^1\mathrm{H}) = 80\ \mathrm{MHz\cdot \AA^3}; \quad t(^2\mathrm{H}) = 12.29\ \mathrm{MHz\cdot \AA^3}$$
$$t(^{13}\mathrm{C}) = 20\ \mathrm{MHz\cdot \AA^3}; \quad t(^{19}\mathrm{F}) = 75.30\ \mathrm{MHz\cdot \AA^3} \qquad (4)$$
$$|K| = {}^7/_3 \text{ for } Fe^{3+}\ (S = {}^5/_2); \quad {}^4/_3 \text{ for } Fe^{2+}\ (S = 2)$$

When the nucleus interacts with both Fe ions, as it would in a bridging or semi-bridging position, the dipolar interaction depends on the distances to both Fe ions and both K_i in a more complicated, but well-defined fashion.[18,29−32] ENDOR simulations were performed following the algorithms described.[17]

To interpret the ^{19}F hyperfine couplings for a bound TFE and ^{1}H couplings for bound water, a search of the Cambridge Structural Database was performed to determine typical binding geometries. For TFE coordinated to iron (or trifluoroacetic acid which has approximately the same size), sample Fe−F distances for the three fluorine atoms in a single structure range between 3.9 and 5.0 Å. For a TFE bound terminally to one iron ion of H_{mv}, these distances correspond to $T(^{19}F) \approx 5.4-2.5$ MHz if the atom is Fe^{3+} and $T(^{19}F) \approx 2.6-1.1$ MHz for Fe^{2+}. The Fe−O distances to the oxygens of water or hydroxide terminally coordinated to Fe^{3+} and Fe^{2+} are expected to be 1.9 and 2.1 Å, respectively; the Fe−O distances in an Fe−O−Fe bridge are ∼1.8−1.9 Å. Assuming a tetrahedral O geometry, the corresponding Fe−H distances would be ∼2.5−2.6 Å for a bridging hydroxide or water bound to the Fe^{3+} and ∼2.8−2.9 Å for a water bound to Fe^{2+}.

Results and Discussion

EPR. Figure 2 presents the EPR spectra of H_{mv} ($g =$ 1.95(6), 1.86(8), ∼1.76) and H_{mv} to which were added methanol, ethanol, or TFE. As shown previously,[19] coordination of methanol to H_{mv} changes the EPR spectrum ($g =$ 1.95(5), 1.85(5), 1.74), shifting g_2 to a slightly lower value and making it broader at fields higher than g_2. The H_{mv} + ethanol and H_{mv} + TFE samples have almost identical EPR spectra, $g =$ 1.94(2), 1.86(3), ∼1.7, and also differ from those of H_{mv}, though less than that of H_{mv} + MeOH, suggesting that these alcohols, like methanol, may bind to the active site. Slight variations in the spectra of H_{mv} from different preparations have been observed, but the ENDOR spectra from all samples of a given state are the same.

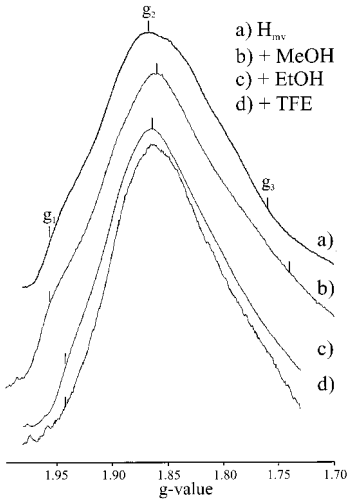

Figure 2. MMOH$_{mv}$ EPR spectra in the presence and absence of substrates: 35.1 GHz MW frequency; modulation amplitude = 1.7 G; $T = 2$ K.

The EPR spectra of $(H_{ox})_{mv}$ and $(H_{ox}$ + MeOH$)_{mv}$ have been reported previously.[20] They are heterogeneous, showing the presence of multiple forms of H_{ox}, one class of which has a rather narrow g-spread ($g =$ 1.95, 1.85, ∼1.75) and the other a larger g-spread ($g =$ 1.94, 1.73, ∼1.6). The spectrum for $(H_{ox}$ + EtOH$)_{mv}$ is qualitatively similar to that of $(H_{ox}$ + MeOH$)_{mv}$; the one for $(H_{ox}$ + EtOH$)_{mv}$ is more homogeneous, comprising primarily a signal with smaller g-anisotropy ($g_2 =$ ∼1.94, $g_z =$ 1.79), similar to that of *p*-nitrophenol and *p*-fluorophenol.[20]

^{1,2}H ENDOR of Exchangeable Protons of H_{mv}. Figure 3 shows 35 GHz CW ^{1}H ENDOR spectra collected at g_2 for H_{mv} in H_2O and D_2O buffer, and for H_{mv} in H_2O to which the several alcohols of interest have been added. The contributions from exchangeable protons have been visualized both by comparison of the ^{1}H spectra of the mixed-valence center in H_2O and D_2O buffers and by direct detection in 35 GHz ^{2}H pulsed ENDOR. Both modes are illustrated in Figure 3 for H_{mv} + TFE.

Our earliest investigation showed that the H_{mv} center exhibits ENDOR signals from the exchangeable proton of the hydroxo-bridge.[33] At g_2 this signal extends out to almost 30 MHz (not shown), but only a small fraction of the intensity of the exchangeable signals in the narrowed frequency range of Figure 3 arises from the bridge. As first found for H_{mv} and H_{mv} + MeOH,[19,33] in each case the spectra show a strong signal from exchangeable proton(s) with splitting $A^H \approx 8$ MHz ($\nu_{+/-} = \nu_H \pm A/2$, where A is the hyperfine coupling), which is ascribed to terminally bound water.[33] Binding of methanol to H_{mv} does not displace this water, as shown previously;[19] Figure 3 shows that

(29) Willems, J.-P.; Lee, H.-I.; Burdi, D.; Doan, P. E.; Stubbe, J.; Hoffman, B. M. *J. Am. Chem. Soc.* **1997**, *119*, 9816−9824.
(30) Hendrich, M. P.; Fox, B. G.; Andersson, K. K.; Debrunner, P. G.; Lipscomb, J. D. *J. Biol. Chem.* **1992**, *267*, 261−269.
(31) Fiege, R.; Zweygart, W.; Bittl, R.; Adir, N.; Renger, G.; Lubitz, W. *Photosynth. Res.* **1996**, *48*, 227−237.
(32) Randall, D. W.; Gelasco, A.; Caudle, M. T.; Pecoraro, V. L.; Britt, R. D. *J. Am. Chem. Soc.* **1997**, *119*, 4481−4491.
(33) DeRose, V. J.; Liu, K. E.; Kurtz, D. M., Jr.; Hoffman, B. M.; Lippard, S. J. *J. Am. Chem. Soc.* **1993**, *115*, 6440−6441.

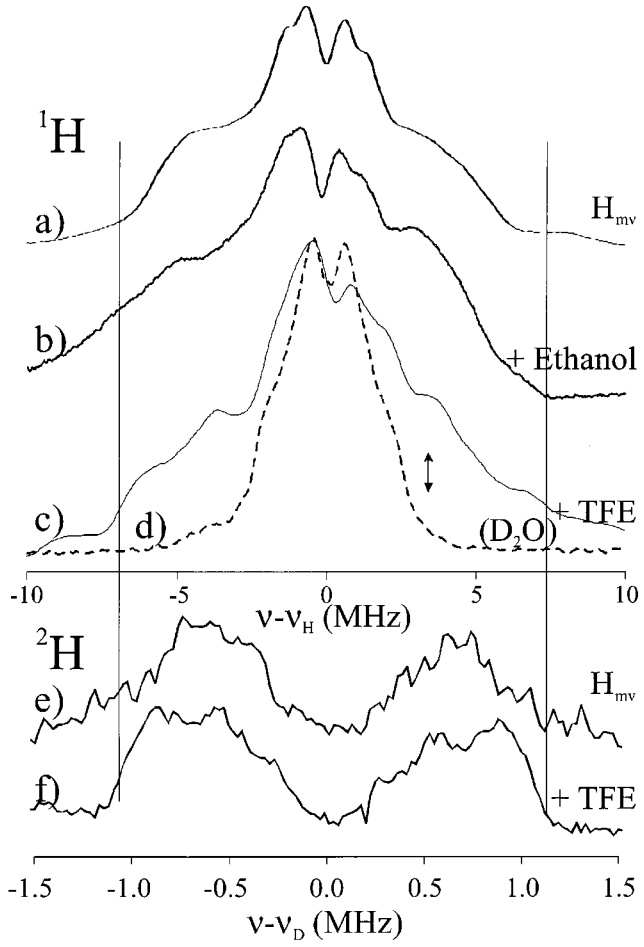

Figure 3. ^{1}H ENDOR spectra of H_{mv}, as well as H_{mv} in the presence of TFE, ethanol, or methanol. The spectrum of the sample exchanged in D_2O is representative of that of H_{mv}, as well as in the presence of the alcohols. **(a)** 35.02 GHz MW frequency, $g = 1.87$; negative scan direction; scan speed 1 MHz/s; 200 kHz (full width) broadening of rf excitation; modulation amplitude = 1.3 G. **(b)** As in (a) but 35.06 GHz, $g = 1.862$; modulation amplitude = 1.7 G; scan speed 1 MHz/s. **(c)** As in (a) but 35.105 GHz MW frequency, $g = 1.840$; negative scan direction; scan speed 2 MHz/s; modulation amplitude = 4.2 G. **(d)** As in (a) but 35.048 GHz MW frequency, $g = 1.841$; positive scan direction; scan speed 1 MHz/s; modulation amplitude = 1.7 G. **(e)** Re-Mims (four-pulse) sequence[28] with a $\pi/2$ microwave pulse = 32 ns, with 20 μs rf pulse and $\tau = 164$ ns; no rf excitation broadening; 34.836 GHz MW frequency, $g = 1.86$; pulse sequence repetition time = 20 ms; 30 averaged data shots per point; 40 scans. **(f)** As in **(e)** but 35.051 GHz MW frequency; pulse sequence repetition time 20 ms; 30 averaged data shots per point; 8 scans.

the same is true for the binding of ethanol and TFE. The ^{1}H H_{mv} + TFE spectrum does show better resolution of some features with $A \approx 13$ MHz, an effect also observed upon the addition of DMSO,[18] but the features are present in the other spectra as well.

Our earlier discussions of this bound water were based on the simple assumption that a terminal water binds with an Fe−O distance of r(Fe−O) ≈ 2 Å. In this case, the main intensity from exchangeable protons in the g_2 spectrum of H_{mv} and of H_{mv} + methanol, with $A \approx 8$ MHz, was best assigned to the "perpendicular" feature, with $|A| \approx T$ (eq 3), for a terminal water bound to Fe^{2+}.

The crystallographic investigation of H_{mv} carried out concurrently with the present ENDOR studies[12] confirms that H_{mv} indeed binds water but indicates that the hydroxo-bridged diiron site binds two H_2O ligands. These waters nominally bind to a single iron ion (Fe1),[12] with this Fe being six-coordinate while the other iron (Fe2) can be three-, four-, or five-coordinate, varying with shifts of the carboxylate of Glu243 (Figure 1).[12] For H_{mv} and for H_{mv} plus each of the alcohols, comparison of the CW ENDOR spectra taken in H_2O and D_2O at g_2 demonstrates that at least one, and probably both, of the water molecules remain coordinated to the center upon binding an alcohol.

It is intuitively appealing to assign the six-coordinate Fe seen in the structure as being the ferric ion. Normally ^{1,2}H ENDOR is an ideal way to test this inference, through the dependence of the dipolar interaction parameter ($T_i^{(H)}$) of the water protons on the valence of the coordinating iron, eq 3. However, the crystal structure indicates that the waters are not 'simple' terminal ligands, but rather are 'semi-bridging' and do not have typical Fe−O distances. For example, the oxygen atom of one water in protomer 1 nominally occupies position 3 (Figure 1), but with an Fe1−O distance of 2.5 Å and an Fe2−O distance of 3.1 Å. Thus, the dipole interaction of the water protons with each Fe is less than for a typical distance. Indeed, a proton on an Fe^{3+}-bound water located at the crystallographic r(Fe−O) distance would exhibit essentially the same T as would a proton on a water bound to Fe^{2+} at a typical distance. As a result, the expected ENDOR patterns for protons associated with the crystallographically characterized waters are not sensitive to the valence assignment as would be the case if the assumptions of terminal binding and typical Fe−O bond distances held.[34]

An attempt to analyze two-dimensional (2D), orientation-selective, field-frequency plots comprising numerous ^{2}H Mims pulsed ENDOR spectra collected across the EPR envelope of H_{mv} (Supporting Information) was thwarted by the task of locating the four water protons in each of the two nonidentical protomers, self-consistently and uniquely, along with the determination of the valency assignment.

^{1,2}H ENDOR measurements on the alcohol-bound H_{mv} center showed that the patterns for the exchangeable protons are very similar to those for H_{mv}, and include contributions both from bound water and the OH^- bridge. Consideration of 2D ENDOR patterns (Supporting Information) indicates that replacement of a water by a protonated bridging alcohol is unlikely but does not discriminate among other possibilities, such as replacement of terminal waters by an alcohol in the same position, or replacement of a water by a deprotonated bridging alcohol.

ENDOR of Nonexchangeable ^{1,2}H of Alcohols Bound to H_{mv}. To examine the binding of ethanol and TFE to H_{mv}, and if possible to determine the binding site, Fe(II) or Fe(III), and geometry (terminal, bridging), we performed Q-band Mims pulsed ^{2}H ENDOR measurements on H_{mv} + CD_3CD_2OH and H_{mv} + CF_3CD_2OH, and compared them to similar results for H_{mv} + CD_3OH.[19] As seen in Figure 4, H_{mv} + CD_3CD_2OH shows a poorly resolved ^{2}H ENDOR doublet signal that is slightly more intense but of similar shape to that of the Fe(II)-bound CD_3OH of H_{mv} + CD_3OH [$A(^2H) \approx 0.5$ MHz, corresponding to $A(^1H) \approx 3.3$ MHz].[19] Moreover, the 2D pattern of field-dependent ^{2}H spectra for H_{mv} + CD_3CD_2OH (Figure S1) is identical with that previously obtained for H_{mv} + CD_3OH.[19] Therefore, the same analysis applies, and we conclude that

(34) The crystal structure, at 2.07 Å resolution, of course does not visualize the protons and thus does not provide additional metrical parameters for analyzing the spectra.

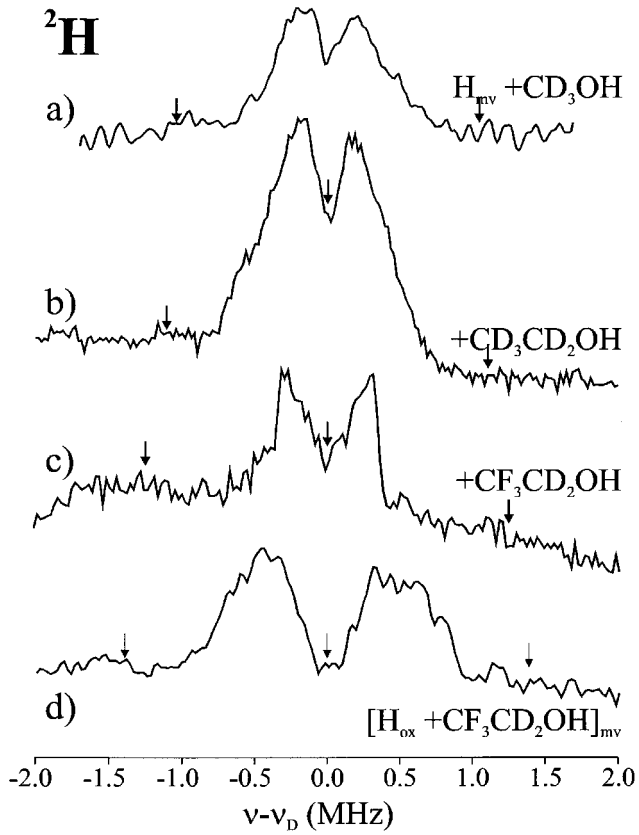

Figure 4. ^{2}H 35 GHz Mims ENDOR of H_{mv}, to which CD_3OH, or CD_3CD_2OH, or CF_3CD_2OH have been added, and of $(H_{ox} + CF_3CD_2OH)_{mv}$; ^{2}H Mims suppression holes are marked on each spectrum. **(a)** $H_{mv} + CD_3OH$ at *g*. $g_2 = 1.86$.[19] **(b)** Mims sequence with a $\pi/2$ microwave pulse = 50−52 ns, with 60 μs rf pulse, $\tau = 452$ ns; 34.695 GHz MW frequency, $g = 1.864$; pulse sequence repetition time = 25 ms; 40 averaged data shots per point; 8 scans; the seventh proton harmonic at 8.09 MHz (−0.6 MHz in the figure) causes a slight asymmetry in this spectrum. ($^H\nu_L = 56.62$ MHz). **(c)** As in (b) but $\tau = 400$ ns; no broadening of rf excitation; 34.594 GHz MW frequency, $g = 1.84$; pulse sequence repetition time = 20 ms; 30 averaged data shots per point; 10 scans. **(d)** As in (b) but Mims sequence with 60 μs rf pulse and $\tau = 360$ ns; 34.584 GHz MW frequency; pulse sequence repetition time = 20 ms; 11 scans.

ethanol, like methanol, coordinates through oxygen to an Fe atom of the H_{mv} diiron core. An assumption of normal Fe−O bond length leads to the suggestion that MeOH binds to the Fe(II), and the same argument would apply to ethanol. Although a semi-bridging structure with the alcohol closer to Fe(II), rather than Fe(III), cannot be excluded, comparison between these results and those reported below for perdeuterated EtOH bound to H_{ox} support the assignment that CD_3CD_2OH is a terminal ligand to Fe^{2+} in H_{mv}. When the same measurements were made with $H_{mv} + CF_3CD_2OH$, a ^{2}H doublet signal was observed (Figure 4), indicating that TFE also binds. The coupling is ∼0.8 MHz.

DMSO coordinates to the Fe(III) iron of H_{mv} and changes its EPR spectrum without displacing bound methanol.[19] Addition of DMSO to H_{mv} + ethanol changed the EPR spectrum to that characteristic of H_{mv} + DMSO, but similarly did not eliminate the ^{2}H ENDOR signal from CD_3CD_2OH. Thus, as with methanol, ethanol can bind simultaneously to H_{mv} with DMSO.

ENDOR of Nonexchangeable ^{1,2}H of Alcohols Bound to $(H_{ox})_{mv}$. To examine the binding of ethanol and TFE to H_{ox}, we added the deuterated alcohols to the enzyme in H_2O buffer, cryoreduced the enzyme, and examined the resulting state by ENDOR spectroscopy. The samples $(H_{ox} + CD_3CD_2OH)_{mv}$ (data not shown) and $(H_{ox} + CF_3CD_2OH)_{mv}$ (Figure 4) both give well-resolved ^{2}H ENDOR signals, clearly indicating that ethanol and TFE bind to H_{ox}. The hyperfine couplings are almost double those for $H_{mv} + CD_3OH$ and the $H_{mv} + CD_3CD_2OH$ complexes throughout a set of spectra at multiple fields (Figure S5). If we assume that the alcohols bind with comparable Fe−O bond lengths in both H_{mv} and H_{ox}, then according to eq 3, one may self-consistently conclude that the smaller couplings for the H_{mv} + alcohol complexes reflect binding to the ferrous ion as suggested above, whereas the larger ^{2}H couplings for the alcohol complexes of the latter are compatible with alcohol binding to H_{ox} in the semi-bridging fashion (Position 3/4, Figure 1) found crystallographically for crystals prepared by diffusion of methanol or ethanol into crystalline H_{ox}.[22]

^{19}F ENDOR. ^{19}F ENDOR of isotopically labeled TFE (CF_3CD_2OH) provides a new probe of the geometry of small-molecule binding to a metalloenzyme active site when the microwave frequency is sufficiently high. At X band the difference between the ^{19}F and ^{1}H Larmor frequencies is very small, less than 1 MHz. As a result, the respective ^{19}F and ^{1}H ENDOR signals would overlap completely for almost any protein sample. At 35 GHz, the difference between the ^{19}F and ^{1}H Larmor frequencies is more than 3 MHz at $g = 2$, although in H_2O buffer, the signals are barely distinguishable from the baseline and often obscured by strongly coupled protons. It is possible, however, to resolve ^{19}F signals from TFE in 35 GHz CW ENDOR spectra collected from a sample that is prepared in D_2O buffer and thus does not exhibit the broad ^{1}H ENDOR signals from the bound water shown in Figure 3. Far better results are obtained, however, through use of the Mims/Re-Mims Q-band pulsed ENDOR technique, and in this case it is *not* necessary to use D_2O buffers. A comparison of the ^{19}F signal obtained in CW or pulsed ENDOR is presented in Figure S4. This pulsed-ENDOR approach allowed us to prepare a single sample with deuterated TFE (CF_3CD_2OH) in H_2O buffer, and to examine both its ^{19}F and nonexchangeable ^{2}H ENDOR responses. For ease of presentation, we first discuss results for $(H_{ox} + CF_3CD_2OH)_{mv}$, then for $(H_{mv} + CF_3CD_2OH)$.

^{19}F ENDOR of $(H_{ox}$ + TFE$)_{mv}$. Figure 5A shows 35 GHz Mims pulsed ENDOR spectra of $(H_{ox} + CF_3CD_2OH)_{mv}$ at several values of τ. The arrows in the figures indicate the Mims "suppression holes" in the spectra, the minima of the sinusoidal Mims response function, eq 2.[35] In all cases, the highly visible ^{1}H signals that extend to $A(^1H) = 8-10$ MHz, in the CW spectra of Figure 2, are diminished in intensity relative to signals with smaller coupling by Mims suppression effects. The more strongly coupled ^{1}H signals are not gone, however. This is best seen in the portion of the $\tau = 228$ ns spectrum with $\nu > \nu_H$, which shows a low-intensity "scalloped" shape given by ^{1}H suppression holes in ^{1}H ENDOR signals from the bound water.

This Mims suppression of ^{1}H signals unmasks the ^{19}F signals, indicated in Figure 5A, which are *not* mirrored to the high-frequency side of ν_H, as ^{1}H signals would be.[36] The Supporting

(35) An anonymous reviewer suggested that we show curves for both the proton and fluorine response functions superimposed on each spectrum; the approach we adopt keeps the spectra distinct and focuses attention to the points where one signal is absent and another one may be present.

(36) A technical comment is in order regarding the spectrum-by-spectrum analysis of Mims pulsed ENDOR data in Figure 5, A and B. It might appear that the simpler alternative for determining the line shape would be to use a "skyline" plot, where one overlays spectra with different τ values. In

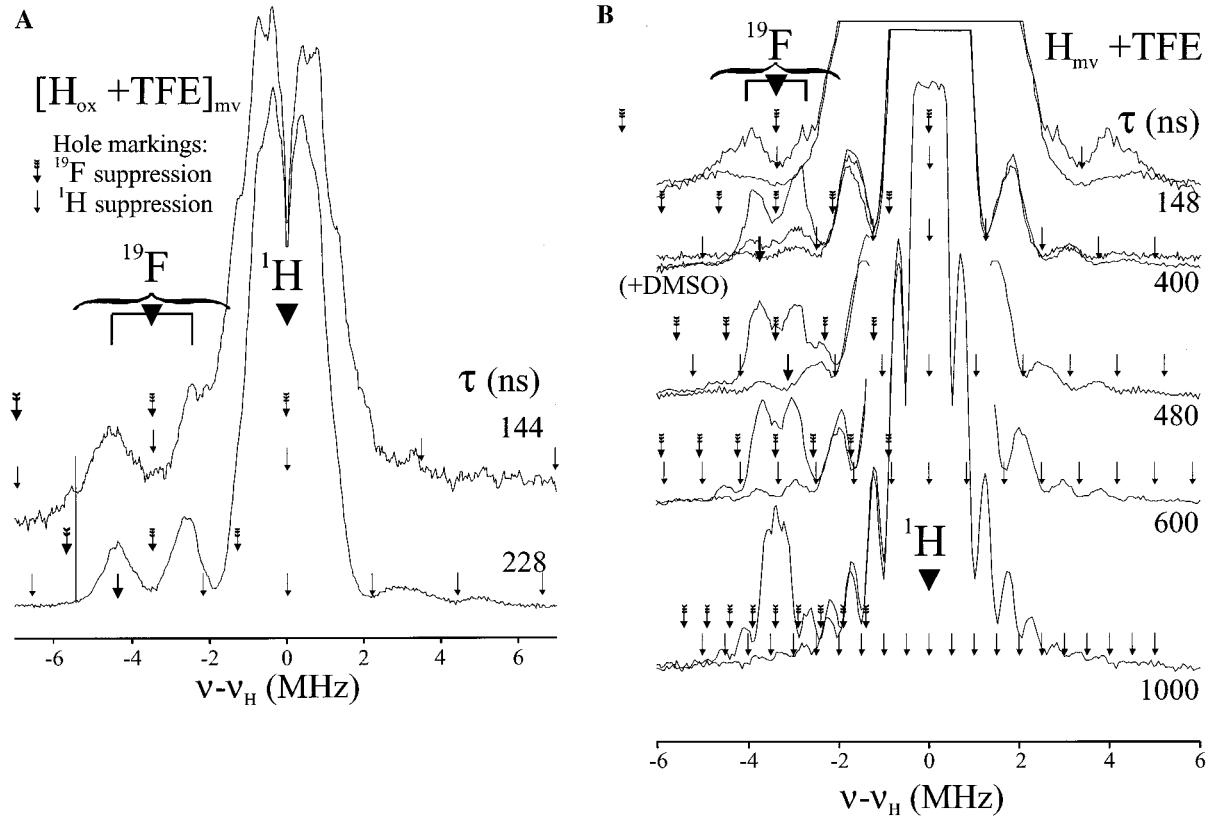

Figure 5. (A) $(H_{ox} + CF_3CD_2OH)_{mv}$ − *J*-dependence of the $^1H/^{19}F$ ENDOR signal. All spectra taken on a sample containing DMSO, except as indicated for the last (bottom) spectrum (without DMSO). Arrows indicate Mims suppression holes, normal and feathered arrows refer to the proton and fluorine signals, respectively. Some arrows are addressed in the text and are printed in boldface for ease of finding them. The spectra are identified by τ: (144 ns) Re-Mims (four-pulse) sequence[28] with a $\pi/2$ microwave pulse = 32 ns, with 20 μs rf pulse, τ = 144 ns; 34.720 GHz MW frequency, g = 1.776; pulse sequence repetition time = 5 ms; 200 averaged data shots per point; 10 scans. (228 ns) As in (144 ns) but τ = 228 ns. (B) H_{mv} + TFE − τ-dependence of the proton/fluorine spectra. All spectra were taken on a sample NOT containing DMSO except as indicated for one of the spectra with τ = 400. (148 ns) Re-Mims (four-pulse) sequence[28] with a $\pi/2$ microwave pulse = 32 ns, with 20 μs rf pulse, τ = 148 ns; 34.638 GHz MW frequency, g = 1.840; pulse sequence repetition time = 25 ms; 40 averaged data shots per point; 20 scans. (400 ns) Mims sequence with a $\pi/2$ microwave pulse = 50−52 ns, with 20 μs rf pulse, τ = 400 ns; 34.596 GHz MW frequency, g = 1.840; pulse sequence repetition time = 25 ms; 40 averaged data shots per point; 3 scans. (400 ns + DMSO) As in (400 ns) but spectrum of H_{mv} + TFE + DMSO, τ = 412 ns; 34.741 GHz MW frequency, pulse sequence repetition time = 30 ms; 30 averaged data shots per point; 2 scans; (overlaid with (400 ns) spectrum). (480 ns) As in (400 ns) but τ = 480 ns; 1 scan; (600ns) As in (400 ns) but τ = 600 ns; 2 scans; (1000 ns) As in (400 ns) but τ = 1000 ns; 5 scans.

Information contains spectra (Figure S8) showing that the ^{19}F signal is unchanged by DMSO binding. The two spectra in Figure 5A reveal how the appearance of the ^{19}F signals is sensitive to τ. With τ = 228 ns, a ^{19}F doublet centered at ν_F and split by an apparent coupling of $A \approx 2$ MHz is clearly seen. In the spectrum with τ = 144 ns, the $\nu_+(^{19}F)$ branch is largely obscured by ^1H signals because the latter are not so fully suppressed, but one can see that the ^{19}F intensity actually spreads over a broader range of frequencies, corresponding to maximum couplings of $A(^{19}F) \approx 4-5$ MHz. In the τ = 228 ns spectrum, the tails of the ^{19}F signals are suppressed.[37]

such a plot one might anticipate that parts of the signal suppressed in one spectrum would be supplied by intensity not suppressed in another one, and that a "true" line shape would result. However, this approach is not useful for samples with substantial envelope modulation or with matrix ENDOR effects. The ESEEM effect produces a different echo height at different τ values, and thus it is not possible to compare absolute intensities meaningfully. The line shape of the signal changes for longer τ values, which enhance matrix/distant ENDOR signals which are centered at the Larmor frequency and which grow and can eventually swamp the local ENDOR signals as τ increases [Astashkin, A. et al. *J. Magn. Res.* **1998**, *135*, 406−417]. Last, we note that experiments at even higher microwave frequencies will further separate the proton and fluorine signals, likely making the use of fluorine as a probe even more convenient and useful.

(37) Illustration of the different patterns of Mims suppression holes in spectra with a wide range of τ, according to eq 2, is presented in the Supporting Information.

^{19}F ENDOR spectra also were taken over a range of magnetic fields to produce a 2D field-frequency plot (Figure S2); they reveal splittings of the main ^{19}F intensities, similar to the ones shown in Figure 5A. The expected "through-space" dipolar coupling for an Fe−F distance of 3.9−5.0 Å is 5.4−2.5 MHz if the Fe atom is Fe^{3+} and 2.6−1.1 MHz (1.6−0.4 MHz axial) for Fe^{2+}. The ^{19}F 2D-plot (Figure S2) reveals a moderate amount of anisotropy in the ^{19}F hyperfine coupling, but due to the presence of multiple Mims suppression holes and the partial overlap with the ^1H signal, it is not possible to determine unambiguously whether the ^{19}F hyperfine interaction contains a substantial isotropic component. Therefore, these data alone do not yield a structural model for the bound TFE. Because the data for H_{mv} + TFE show much smaller ^{19}F couplings, however, we self-consistently interpret them with a model where TFE binds to the $(H_{ox} + TFE)_{mv}$ at the Fe^{3+} ion, or in a bridging mode (see below).

^{19}F ENDOR of H_{mv} + TFE. Analogous ^{19}F ENDOR measurements were made with $H_{mv} + CF_3CD_2OH$, and Figure 5B shows ^{19}F Mims and Re-Mims pulsed ENDOR spectra collected at g_2 at several values of τ. As in Figure 5A, the portion of the spectrum with $\nu > \nu_H$ shows a low-intensity "scalloping"

given by ^{1}H suppression holes in the ^{1}H ENDOR signals from the bound water. Again, the suppression of the water proton signal discloses a ^{19}F doublet centered around ν_F, with the suppression pattern confirming the assignment of this doublet to ^{19}F. In the top, Re-Mims, spectrum, with $\tau = 148$ ns, the short τ places the ^{19}F suppression holes well outside the ^{19}F intensity; the doublet splitting appears to be roughly $A \approx 1.3$ MHz, with the ν_+ peak being largely hidden under the proton signal intensity.

The $\tau = 400$ and 480 ns Mims ENDOR spectra respectively place a proton suppression hole at the ν_- and ν_+ peaks of the doublet assigned to ^{19}F. The fact that this doublet is not suppressed confirms that the intensity is indeed due to ^{19}F. From these two spectra we conclude that a somewhat better value for the ^{19}F hyperfine coupling is $A \approx 1$ MHz, roughly half that in $(H_{ox} + TFE)_{mv}$, as is the case for the ^{2}H couplings. Thus, with the assumption of standard bond lengths, the ^{19}F ENDOR measurements of TFE are consistent with the ^{1,2}H measurements of MeOH and EtOH. The alcohols bind terminally to the ferrous ion of H_{mv}, while binding in a bridging or semi-bridging fashion to H_{ox}, as found crystallographically for the MeOH complex of H_{ox}.[22,38]

DMSO Binding to H_{mv} (+ Alcohols). The $\tau = 400$ spectrum in Figure 5B is overlaid with a trace from a H_{mv} sample that contains both DMSO and TFE, which has an EPR spectrum that is the same as that reported for H_{mv} + DMSO. The ^{19}F signal seen for H_{mv} + TFE is eliminated, however, by the addition of DMSO, while the ^{1}H signals remain identical. Overlays of the ν_+ proton intensity over the ν_- peaks shows that some of the intensity left over in the region around ν_F is actually proton intensity, with less than 20% of it due to ^{19}F signals. Although the elimination of TFE is not complete, this result indicates that DMSO binding to the Fe(III) ion of H_{mv} prevents most of the TFE binding that occurs in the absence of DMSO. This competition between DMSO and TFE contrasts with the observation that DMSO binding to the Fe(III) of H_{mv} does not preclude methanol[19] or ethanol binding to Fe(II).

Conclusions

The present study has combined ^{1,2}H and ^{19}F ENDOR measurements to examine ethanol and TFE bound to both the H_{ox} and H_{mv} diiron centers of solution MMOH and has compared these results to those from X-ray diffraction studies of preformed crystals into which alcohol had been diffused. In the process we have introduced ^{19}F ENDOR spectroscopy as a valuable complement to the use of ^{1,2}H ENDOR spectroscopy in probing the structure of substrates or products bound to catalytic metal centers in enzymes. The ^{1,2}H ENDOR spectra of d_5-ethanol and of d_2-TFE, and the ^{19}F ENDOR of TFE obtained for the alcohols bound to solution H_{ox}, as visualized by cryoreduction to $(H_{ox})_{mv}$, are compared with those for the alcohols as bound to H_{mv} prepared in solution. The results, as interpreted in terms of eq 3, indicate that the alcohols bind close to Fe(II) of the EPR-active, mixed-valence cluster of H_{mv}, either in a terminal or semi-bridging fashion, as previously suggested for MeOH.[19] They bind to H_{ox} in a bridging, or semi-bridging fashion closer to the Fe^{3+} ion of $(H_{ox})_{mv}$, consistent with crystallographic structures for complexes prepared by diffusion of alcohols into preformed crystals of H_{ox}.[22] The early proposal that alcohols bind to the diiron(III) state in a bridging mode and distal to the histidine ligands in the active-site cavity (positions 3 and 4, in Figure 1),[9] is thus strongly supported by the crystallographic result obtained from alcohol-treated H_{ox} crystals,[22] by the ENDOR studies on the enzyme in solution, and by recent density functional calculations[39] on the reaction of methane with intermediate Q. ^{1,2}H ENDOR spectra of exchangeable protons further suggest that the ethanols, like methanol,[19] bind to H_{mv} without replacing coordinated water. Detailed examination of the ^{2}H ENDOR spectra of H_{mv} and H_{mv} + ethanol shows that the structural flexibility of the diiron centers (illustrated by differences in the crystal structure protomers) precludes an in-depth analysis, but the data are consistent with the crystallographic result[12,22] that two waters bind weakly to one of the Fe ions of H_{mv}.

DMSO does not affect the binding of either of the ethanols or of methanol to H_{ox}, nor of ethanol or methanol to H_{mv}. It does, however, displace TFE from the diiron site in H_{mv}, a difference consistent with the weaker coordinating ability of this alcohol owing to the electron-withdrawing fluorine atoms.

Acknowledgment. This work was supported by NIH Grants HL13531 (to B.M.H.) and GM32134 (to S.J.L.). D.A.K. is a National Institutes of Health biotechnology predoctoral trainee.

Supporting Information Available: Additional ^{2}H and ^{19}F ENDOR data (Figures S1−S5); a discussion of the analysis of ^{2}H ENDOR spectra of exchangeable protons illustrated with field-dependent ^{2}H spectra (Figure S6); pulsed ^{1}H/^{19}F Mims ENDOR of H_{mv} + hexafluoro-2-propanol (Figure S7); J-dependence of the ^{1}H/^{19}F ENDOR signal in $(H_{ox} + CF_3CD_2OH)_{mv}$ (Figure S8) (PDF). This material is available free of charge via the Internet at http://pubs.acs.org.

JA010123Z

(38) Note again, however, if bond lengths vary appreciably, other options may become plausible.

(39) Gherman, B. F.; Dunietz, B. D.; Whittington, D. A.; Lippard, S. J.; Friesner, R. A. *J. Am. Chem. Soc.* **1993**, *115*, **2001**, *123*, 3836−3837.